Available online at www.sciencedirect.com
SCIENCE DIRECT®
Pergamon
Acta Materialia 51 (2003) 5499–5518
Acta MATERIALIA
www.actamat-journals.com

A level set method for dislocation dynamics

Yang Xiang [a,*], Li-Tien Cheng [b], David J. Srolovitz [c], Weinan E [d]

[a] *Princeton Materials Institute, Princeton University, Bowen Hall, 70 Prospect Avenue, Princeton, NJ 08544, USA*
[b] *Department of Mathematics, University of California, San Diego, La Jolla, CA 92093, USA*
[c] *Princeton Materials Institute and Department of Mechanical and Aerospace Engineering, Princeton University, Princeton, NJ 08544, USA*
[d] *Department of Mathematics and PACM, Princeton University, Princeton, NJ 08544, USA*

Received 23 May 2003; received in revised form 17 July 2003; accepted 19 July 2003

Abstract

We propose a three-dimensional level set method for dislocation dynamics in which the dislocation lines are represented in three dimensions by the intersection of the zero levels of two level set functions. Since the level set method does not discretize nor directly track individual dislocation line segments, it easily handles topological changes occurring in the microstructure. The dislocation dynamics are not limited to glide along a slip plane, but also account for three-dimensional aspects of their motion: cross-slip occurs naturally and climb is included by fixing the relative climb and glide mobility. The level set dislocation dynamics method was implemented using an accurate finite difference scheme on a uniform grid. To demonstrate the versatility, utility and simplicity of this new model, we present examples including the motion of dislocation loops under applied and self-stresses (including glide, cross-slip and climb), intersections of dislocation lines, operation of Frank–Read sources and dislocations bypassing particles.

Keywords: Dislocation dynamics; Modelling; Simulation

1. Introduction

Although dislocation theory began in the early years of the last century and has been an active area of investigation ever since (see Refs. [1–3]), our ability to describe the evolution of dislocation microstructures has been limited by the inherent complexity of the problem. This complexity is associated with several contributing features. The interactions between dislocations are extraordinarily long-ranged and depend on the relative positions of the dislocations, the orientation of their Burgers vectors (i.e. vector strength) and line orientating. Dislocation mobility depends on the orientations of the Burgers vector and line direction with respect to the crystal structure. A description of the dislocation structure within a solid is further complicated by such topological events as annihilation, multiplication and reaction. As a result, analytical descriptions of dislocation structure have been limited to a small number of simple geometrical configurations. More recently, several dislocation dynamics simulation methods have

* Corresponding author. Tel.: +1-609-258-0494; fax: +1-609-258-6878.
E-mail address: yxiang@princeton.edu (Y. Xiang).

1359-6454/$30.00
doi:10.1016/S1359-6454(03)00415-4

been developed that account for complex dislocation geometries and/or the motion of multiple, interacting dislocations (see e.g. [4–13]). This approach is becoming an increasingly important tool for describing plastic deformation.

The existing models for dislocation dynamics can be divided into two main classes. The first is based upon front tracking methods, in which dislocation lines are discretized into individual segments. During these simulations, each segment is tracked and the force on each segment from all other segments are calculated at each time increment (usually using the Peach–Koehler formula [14]). Early front tracking simulations focused on the motion of a single dislocation on its slip plane (i.e. the plane containing the Burgers vector and the line direction) interacting with obstacles [15–17]. Kubin and coworkers performed mesoscopic three-dimensional simulations of multiple dislocations [4,5,18]. In their model, dislocation lines are discretized into straight, pure edge and screw segments. More recently, other researchers represented dislocation lines by segments with mixed character [6–8] and/or curved spline segments [9]. Three-dimensional front tracking methods made it possible to simulate dislocations motion with a degree of reality heretofore not possible. However, such methods are necessarily time-consuming, since they track each segment of all dislocation lines and calculate the force acting on it from all other segments at each time increment. Moreover, special rules are needed to describe the topological changes that occur when two segments of the same dislocation annihilate (as in Orowon loop formation) or when two dislocations with the same Burgers vector meet and annihilate [8,9,12]).

Another class of dislocation dynamics models employs a phase field description of dislocations, as proposed by Khachaturyan, Wang and coworkers [10,11]. In their phase field model, density functions are used to model the evolution of a three-dimensional dislocation system. Dislocation loops are described as the perimeters of thin platelets determined by the density functions. Since this method is based upon the evolution of a field in the full dimensions of the space, there is no need to track individual dislocation line segments and topological changes occur automatically. The elastic interactions of the dislocations are determined efficiently using fast Fourier transform (FFT) methods for the case of periodic boundary conditions. However, contributions to the energy that are normally not present in dislocation theory must be included within the phase field model to keep the dislocation core from expanding (i.e. terms that describe Burgers vector gradients, as in Eq. (9) of Ref. [11]). In addition, dislocation climb is not easily incorporated into this type of model.

In this paper, we propose a three-dimensional level set method for dislocation dynamics. We represent dislocation lines in three dimensions as the intersection of the zero levels (or zero contours) of two three-dimensional scalar functions (see Refs. [19–21] for a description of the level set method). The two three-dimensional level set functions are evolved using a velocity field extended smoothly from the velocity of the dislocation lines. The evolution of the dislocation lines is implicitly determined by the evolution of the two level set functions. Linear elasticity theory is used to compute the stress field generated by the dislocation lines [3,22,23]. The stress field can be solved efficiently using an FFT method, assuming periodic boundary conditions. Since the level set method does not track individual dislocation line segments, it easily handles topological changes associated with dislocation multiplication and annihilation. This level set method for dislocation dynamics is capable of simulating the three-dimensional motion of dislocations, naturally accounting for dislocation glide, cross-slip and climb through the choice of the ratio of the glide and climb mobilities. Unlike previous field-based methods [10,11], no unconventional contributions to the system energy are required to keep the dislocation core localized.

This paper is organized as follows. In Section 2, we review relevant aspects of the continuum theory of dislocations. In Section 3, we describe the general features of the level set method and how we apply it to dislocation dynamics. In Section 4, we discuss the numerical implementation of our level set method for dislocation dynamics. In Section 5, we demonstrate the generality and power of the new method through a series of test applications including the glide, cross-slip and climb of dislo-

cation loops under applied and/or self stresses, interactions between two non-coplanar dislocation lines, operation of a Frank–Read source, and a series of examples of dislocations bypassing particles.

2. Continuum dislocation theory

In this section, we briefly review aspects of the continuum theory of dislocations that are used in the development of the level set description of dislocation dynamics, below. More complete descriptions of the continuum theory of dislocations can be found in, e.g. [2,3,22,23].

Dislocations are line defects in crystals for which the elastic displacement vector satisfies

$$\oint_L \mathrm{d}\mathbf{u} = \mathbf{b} \tag{1}$$

where L is any contour enclosing the dislocation line with Burgers vector $\mathbf{b}$. Note, the elastic displacement vector $\mathbf{u}$ is multi-valued. The Burgers vector $\mathbf{b}$ and dislocation line direction ξ can have any orientation with respect to one another. A dislocation for which these vectors are perpendicular is an edge dislocation and is a screw dislocation if they are parallel. The general case is referred to as a mixed dislocation.

We define the distortion tensor $\mathbf{w}$ in terms of the displacement field u as

$$w_{ij} = \frac{\partial u_j}{\partial x_i} \tag{2}$$

for $i,j = 1,2,3$. We can now rewrite Eq. (1) as

$$\oint_L \mathbf{w}\cdot\mathrm{d}\mathbf{x} = \mathbf{b}. \tag{3}$$

Using Stokes' theorem, we obtain

$$\oint_S \nabla \times \mathbf{w}\cdot\mathbf{n}\,\mathrm{d}S = \oint_L \mathbf{w}\cdot\mathrm{d}\mathbf{x} = \mathbf{b} \tag{4}$$

$$= \mathbf{b}\oint_S \delta(\gamma)\xi\cdot\mathbf{n}\,\mathrm{d}S$$

where S is any surface spanning the contour L, $\mathbf{n}$ is the normal to the surface S, γ is the location of the dislocation line, ξ is the unit vector tangent to the dislocation line, $\delta(\gamma)$ is the two dimensional delta function in the plane perpendicular to the dislocation line and is zero everywhere except on the dislocation line. It is convenient to rewrite Eq. (4) as

$$\nabla \times \mathbf{w} = \xi\delta(\gamma)\otimes\mathbf{b} \tag{5}$$

where the operator $\otimes$ implies the tensor product of two vectors.

While the Burgers vector is constant along any dislocation line, different dislocation lines may have different Burgers vectors. Eq. (5) is valid only for dislocations with the same Burgers vector. In crystalline materials, the number of possible Burgers vectors is finite, N (e.g. typically $N = 12$ for a FCC metal). Eq. (5) may be extended to account for all possible Burgers vectors:

$$\nabla \times \mathbf{w} = \sum_{i=1}^{N} \xi_i\delta(\gamma_i)\otimes\mathbf{b}_i \tag{6}$$

where γ_i represents all of the dislocations with Burgers vector $\mathbf{b}_i$ and ξ_i is the tangent to dislocation line i.

Now we consider the strain and stress tensors associated with the dislocations. The strain tensor is given by

$$\varepsilon_{ij} = \frac{1}{2}(w_{ij} + w_{ji}) \tag{7}$$

for $i, j = 1, 2, 3$. The stress tensor σ is determined from the strain tensor by the linear elastic constitutive equations

$$\sigma_{ij} = \sum_{k,l=1}^{3} C_{ijkl}\varepsilon_{kl} \tag{8}$$

for $i, j = 1, 2, 3$, where $\{C_{ijkl}\}$ is the elastic constant tensor. For an isotropic medium, the constitutive equations can be written as

$$\sigma_{ij} = 2G\varepsilon_{ij} + G\frac{2\nu}{1-2\nu}(\varepsilon_{11} + \varepsilon_{22} + \varepsilon_{33})\delta_{ij} \tag{9}$$

for $i, j = 1, 2, 3$, where G is the shear modulus, ν is the Poisson ratio, and δ_{ij} is equal to 1 if $i = j$ and is equal to 0 otherwise. In the absence of body forces, the equilibrium equation is simply

$$\nabla\cdot\sigma = 0. \tag{10}$$

Finally, the stress and strain tensors associated with a dislocation can be found by combining Eqs. (5), (7), (8) and (10).

Dislocations can move under stress. The Peach–Koehler force on the dislocations is given by

$$\mathbf{f} = \sigma^{\text{tot}}\cdot\mathbf{b} \times \xi \tag{11}$$

where the total stress field σ^{tot} includes the self-stress σ obtained by solving Eqs. (5), (7), (8) and (10), and the applied stress σ^{appl}:

$$\sigma^{\text{tot}} = \sigma + \sigma^{\text{appl}} \tag{12}$$

The local dislocation velocity is given by

$$\mathbf{v} = \mathbf{M}\cdot\mathbf{f} \tag{13}$$

where $\mathbf{M}$ is the mobility tensor.

A dislocation line can move conservatively (i.e. without diffusion) only in the plane containing both its tangent vector and the Burgers vector (i.e. the slip plane). A screw segment on a dislocation line can move in any plane containing the dislocation line, since the tangent vector and Burgers vector are parallel. The switching of a screw segment from one slip plane to another is known as cross-slip. At high temperatures, edge segments of a dislocation can also move out of the slip plane by a non-conservative (i.e. diffusive) process known as climb. The mobility tensor $\mathbf{M}$ is defined such as to account for the relatively high glide mobility and slow climb mobility. The present method is equally applicable to all crystal systems and all crystal orientations through appropriate choice of the Burgers vector and the mobility tensor (which can be rotated into any arbitrary orientation). In the present model, the dislocation can slip on all mathematical slip planes (i.e. planes containing the Burgers vector and line direction) and are not constrained to a particular set of crystal plane $\{h\,k\,l\}$. This restriction will be imposed in later variations of this method.

The self-stress obtained by solving the elasticity Equations (5), (7), (8) and (10) is singular on the dislocation line. This singularity is artificial because of the discreteness of the atomic lattice and non-linearities in the stress–strain relation not included in the linear elastic framework. This non-linear region is called the dislocation core. One approach to handling this problem is to use a smeared delta function instead of the exact delta function in Eq. (5) near each point on the dislocation line. The smeared delta function, like the exact one, is defined in the plane perpendicular to the dislocation line, and the vector ξ is defined everywhere in this plane to be the dislocation line tangent vector. This smeared delta function can be considered to be the distribution of the Burgers vector in the plane perpendicular to the dislocation line. The width of the smeared delta function is the diameter of the core region of the dislocation line. From this point forward, we will use this approach to treat the dislocation core and its smeared delta function description. A necessary condition for the elasticity equation (5) to have a solution is

$$\nabla\cdot(\xi\delta(\gamma)) = 0. \tag{14}$$

Using the local system of coordinates on the dislocation line, it is easy to verify that the smeared delta function and the vector ξ defined in this way satisfy this condition.

3. The level set dislocation dynamics method

In this section, we first briefly review the existing level set framework for the motion of three-dimensional curves and then present our level set approach to dislocation dynamics.

The level set method was devised by Osher and Sethian [19] in 1987 and has been successfully applied to a wide range of problems (as discussed in a recent review [21]). Recently, Burchard et al. [20] presented numerical simulations using a level set approach for moving curves in three-dimensional space. In their model, a three-dimensional curve $\gamma(t)$ is represented by the intersection of the zero levels of two level set functions $\phi(x, y, z, t)$ and $\psi(x, y, z, t)$ defined in the three-dimensional space, i.e. where

$$\phi(x,y,z,t) = \psi(x,y,z,t) = 0, \tag{15}$$

see Fig. 1. The evolution of the curve is described by

$$\begin{aligned} \phi_t + \mathbf{v}\cdot\nabla\phi &= 0 \\ \psi_t + \mathbf{v}\cdot\nabla\psi &= 0 \end{aligned} \tag{16}$$

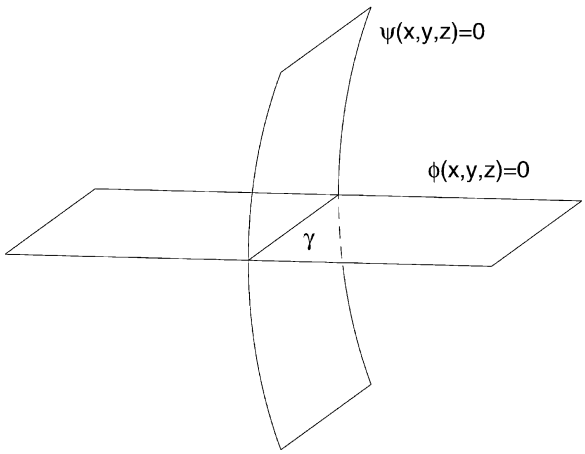

Fig. 1. A three-dimensional curve $\gamma(t)$ is the intersection of the zero levels of the two level set functions $\phi(x, y, z, t)$ and $\psi(x, y, z, t)$.

where **v** is the velocity field extended smoothly from the curve to the three-dimensional space. The reason this system of partial differential equations gives the correct motion of the curve can be understood in the following way. Assume that the curve $\gamma(s, t)$ described in parametric form using the variable s, is given by

$$\begin{aligned}\phi(\gamma(s,t),t) &= 0\\ \psi(\gamma(s,t),t) &= 0,\end{aligned} \tag{17}$$

where t is time. Taking a derivative of Eq. (17) with respect to t gives

$$\begin{aligned}\nabla\phi(\gamma(s,t),t)\cdot\gamma_t(s,t) + \phi_t(\gamma(s,t),t) &= 0\\ \nabla\psi(\gamma(s,t),t)\cdot\gamma_t(s,t) + \psi_t(\gamma(s,t),t) &= 0.\end{aligned} \tag{18}$$

Comparing with Eq. (16), we have

$$\gamma_t(s,t) = \mathbf{v}, \tag{19}$$

which means the velocity of the curve is equal to **v**.

Geometric properties of the curve can be calculated from the level set functions ϕ and ψ. For example, the tangent vector ξ can be written as

$$\xi = \frac{\nabla\phi \times \nabla\psi}{|\nabla\phi \times \nabla\psi|}. \tag{20}$$

In this paper, we use the level set framework for three-dimensional curves to describe dislocation dynamics. In our level set method for dislocation dynamics, the union of the three-dimensional dislocation lines $\gamma(t)$ is represented by Eq. (15) and its evolution is given by Eq. (16). The velocity field of a dislocation is computed from the stress field using Eqs. (11)–(13). The self-stress field is obtained by solving the elasticity equations (5), (7), (8) and (10). The tangent vector ξ in equations (5) and (11) is calculated using Eq. (20).

The above representation applies only to the case where all dislocations have the same Burgers vector **b**. For a more general case where dislocation lines have different Burgers vectors, we can use different level set functions ϕ_i and ψ_i for different Burgers vectors $\mathbf{b}_i$, $i = 1, 2, ..., N$, where N is the total number of the possible Burgers vectors, and use Eq. (6) instead of Eq. (5) in the elasticity equations.

The delta function in Eq. (5) is given by

$$\delta(\gamma) = \delta(\phi)\delta(\psi), \tag{21}$$

where the delta functions on the right-hand-side are one-dimensional, smeared delta functions

$$\delta(x) = \begin{cases} \dfrac{1}{2\varepsilon}\left(1 + \cos\dfrac{\pi x}{\varepsilon}\right) & -\varepsilon \le x \le \varepsilon \\ 0 & \text{otherwise} \end{cases} \tag{22}$$

and ε scales the distance over which the delta function is smeared. The region where the delta-function is not zero represents the core region of the dislocation line. Usually in the level set method, the level set functions ϕ and ψ are chosen to be signed distance functions to their zero levels and their zero levels are kept perpendicular to each other. A procedure called reinitialization is used to retain these properties of ϕ and ψ during their temporal evolution (see the next section for details). Therefore the delta function defined by Eq. (21) is a two-dimensional smeared delta function in the plane perpendicular to the dislocation line. Moreover, the size and the shape of the core region will not change during the evolution.

Now we define the mobility tensor **M**. First note that the normal vector of the slip plane that contains the tangent vector ξ of the dislocation and the Burgers vector **b**, is given by

$$\mathbf{n} = \frac{\xi \times \mathbf{b}}{|\xi \times \mathbf{b}|}. \tag{23}$$

The orthogonal projection matrix that projects vectors onto the plane with normal vector $\mathbf{n}$ is given by

$$\mathbf{P} = \mathbf{I} - \mathbf{n} \otimes \mathbf{n}, \tag{24}$$

where $\mathbf{I}$ is the identity matrix and $\otimes$ is the tensor product operator. We now write the mobility tensor in the general form

$$\mathbf{M} = \tag{25}$$

$$\begin{cases} m_g(\mathbf{I} - \mathbf{n} \otimes \mathbf{n}) + m_c \mathbf{n} \otimes \mathbf{n} & \text{edge } (\xi \text{ not parallel to } \mathbf{b}) \\ m_g \mathbf{I} & \text{screw } (\xi \text{ parallel to } \mathbf{b}) \end{cases}$$

where m_g is the mobility constant for dislocation glide and m_c is the mobility constant for dislocation climb, and

$$0 \le \frac{m_c}{m_g} \le 1. \tag{26}$$

While we implicitly assume that the glide mobilities of edge and screw segments are identical, this assumption is easily relaxed. Unless otherwise noted, we will assume that $m_c = 0$ (i.e. dislocation can only glide) in this paper.

For simplicity, we employ isotropic elasticity throughout this paper. While anisotropy will not cause any essential difficulties in our model, the added complexity clouds the description of the method. If we further assume periodic boundary conditions, the solution of the elasticity equations (5), (7), (9) and (10) takes the form of Eq. (27) below, where $\hat{\sigma}_{ij}$ is the Fourier coefficient of the term $e^{ik_1x + ik_2y + ik_3z}$ for σ_{ij}, $i, j = 1, 2, 3$, $\hat{d}_i$, $i = 1, 2, 3$ are the Fourier coefficients of the term $e^{ik_1x + ik_2y + ik_3z}$ for the three components of $\xi\delta(\gamma)$, respectively, and b_1, b_2, b_3 are the three components of the Burgers vector $\mathbf{b}$.

This solution is valid only for the case where the summation of the total Burgers vector is equal to zero in the simulation cell. If the total Burgers vector is not equal to zero, the stress is equal to a periodic function plus a linear function in x, y and z [24,25]. In this case, we also use the above formula, since it only gives the periodic part of the stress field. This is consistent with the approach suggested by Bulatov, Cai and coworkers for computing periodic image interactions in the front tracking method [24,25].

In summary, in the case of isotropic elasticity with periodic boundary conditions, our level set method for dislocation dynamics consists of the evolution equation (16), the velocity field equations (11)–(13), and the self-stress field equation (27).

4. Numerical implementation

The numerical implementation for our level set dislocation dynamics method consists of two parts. The first is the elasticity part, which involves com-

$$\hat{\sigma}_{11} = 2Gi\left(\frac{1}{k_1^2+k_2^2+k_3^2}(k_2b_3-k_3b_2)\hat{d}_1 - \frac{1}{1-\nu}\frac{k_2^2+k_3^2}{(k_1^2+k_2^2+k_3^2)^2}[(k_2b_3-k_3b_2)\hat{d}_1 + (k_3b_1-k_1b_3)\hat{d}_2 + (k_1b_2-k_2b_1)\hat{d}_3]\right)$$

$$\hat{\sigma}_{22} = 2Gi\left(\frac{1}{k_1^2+k_2^2+k_3^2}(k_3b_1-k_1b_3)\hat{d}_2 - \frac{1}{1-\nu}\frac{k_1^2+k_3^2}{(k_1^2+k_2^2+k_3^2)^2}[(k_2b_3-k_3b_2)\hat{d}_1 + (k_3b_1-k_1b_3)\hat{d}_2 + (k_1b_2-k_2b_1)\hat{d}_3]\right)$$

$$\hat{\sigma}_{33} = 2Gi\left(\frac{1}{k_1^2+k_2^2+k_3^2}(k_1b_2-k_2b_1)\hat{d}_3 - \frac{1}{1-\nu}\frac{k_1^2+k_2^2}{(k_1^2+k_2^2+k_3^2)^2}[(k_2b_3-k_3b_2)\hat{d}_1 + (k_3b_1-k_1b_3)\hat{d}_2 + (k_1b_2-k_2b_1)\hat{d}_3]\right)$$

$$\hat{\sigma}_{12} = \hat{\sigma}_{21} = 2Gi\left(\frac{1}{2(k_1^2+k_2^2+k_3^2)}[(k_3b_1-k_1b_3)\hat{d}_1 + (k_2b_3-k_3b_2)\hat{d}_2] + \frac{1}{1-\nu}\frac{k_1k_2}{(k_1^2+k_2^2+k_3^2)^2}[(k_2b_3-k_3b_2)\hat{d}_1 + (k_3b_1-k_1b_3)\hat{d}_2 + (k_1b_2-k_2b_1)\hat{d}_3]\right)$$

$$\hat{\sigma}_{23} = \hat{\sigma}_{32} = 2Gi\left(\frac{1}{2(k_1^2+k_2^2+k_3^2)}[(k_1b_2-k_2b_1)\hat{d}_2 + (k_3b_1-k_1b_3)\hat{d}_3] + \frac{1}{1-\nu}\frac{k_2k_3}{(k_1^2+k_2^2+k_3^2)^2}[(k_2b_3-k_3b_2)\hat{d}_1 + (k_3b_1-k_1b_3)\hat{d}_2 + (k_1b_2-k_2b_1)\hat{d}_3]\right)$$

$$\hat{\sigma}_{13} = \hat{\sigma}_{31} = 2Gi\left(\frac{1}{2(k_1^2+k_2^2+k_3^2)}[(k_1b_2-k_2b_1)\hat{d}_1 + (k_2b_3-k_3b_2)\hat{d}_3] + \frac{1}{1-\nu}\frac{k_1k_3}{(k_1^2+k_2^2+k_3^2)^2}[(k_2b_3-k_3b_2)\hat{d}_1 + (k_3b_1-k_1b_3)\hat{d}_2 + (k_1b_2-k_2b_1)\hat{d}_3]\right) \tag{27}$$

puting the velocity field in the evolution equation (16) from the elasticity theory, including Eqs. (11)–(13) and (27). The second is the level set part, which involves solving the evolution equation (16) and maintaining good level set functions using level set techniques such as reinitialization and velocity interpolation and extension.

4.1. Computing elastic fields

We solve the elasticity equations associated with the dislocations using the FFT approach, as given by Eq. (27). First step is to compute the dislocation tangent vector $\xi\delta(\gamma)$ from the level set functions ϕ and ψ. The delta function $\delta(\gamma)$ is computed using Eq. (21) with core radius $\varepsilon = 3\mathrm{d}x$, where $\mathrm{d}x$ is the spacing of the numerical grid. The tangent vector ξ is computed using a regularized form of Eq. (20) (to avoid division by zero), i.e.

$$\xi = \frac{\nabla\phi \times \nabla\psi}{\sqrt{|\nabla\phi \times \nabla\psi|^2 + \mathrm{d}x^2}}, \tag{28}$$

as is standard in level set methods.

The gradients of ϕ and ψ in Eq. (28) are computed using the third order WENO method [26]. Since WENO derivatives are one-sided, we switch sides after several time steps to reduce the error caused by asymmetry. The reason that one-sided derivatives are used instead of a centered one is as follows. The leading order effect of the self-stress of the dislocation is associated with dislocation curvature [3,22], which tends to stabilize high frequency oscillations of the dislocation line. If we use central differencing to compute the derivatives, the formulation for the self-stress will not see the high frequency oscillations and therefore does not give the correct self-stress needed to stabilize the dislocation lines.

After we obtain the self-stress, we compute the velocity field using Eqs. (11)–(13). We now use central differencing to compute the gradients of ϕ and ψ in Eq. (28) to get the tangent vector ξ in Eqs. (11) and (23). The mobility tensor in Eq. (13) is computed using Eqs. (23) and (25). We also regularize the denominator in Eq. (23) to avoid division by zero, as we did in Eq. (28). For the mobility tensor (Eq. (25)), we use the mobility for a screw dislocation when $|\xi \times \mathbf{b}| < 0.1$ and use the mobility for an edge dislocation otherwise (see Eq. (25)).

4.2. Numerical implementation of the level set method

4.2.1. Solving the evolution equations

The level set evolution equations are commonly solved using high order ENO (essentially nonoscillatory) or WENO (weighted essentially nonoscillatory) methods for the spatial discretization [19,26,27] and TVD (total variation diminishing) Runge–Kutta methods for the time discretization [28,29]. In this paper, we compute the spatial upwind derivatives using the third order WENO method [26] and use fourth order TVD Runge–Kutta [29] to solve the temporal evolution equation (16).

4.2.2. Reinitialization

In level set methods for three-dimensional curves, the desired level set functions ϕ and ψ are signed distance functions to their zero levels (i.e. the value at each point in the scalar field is equal to the distance from the closest point on the zero level contour surface with a positive value on one side of the zero level and a minus sign on the other). Ideally, the zero level surfaces of these two functions should be perpendicular to each other. Initially, we choose ϕ and ψ to be such signed distance functions. However, there is no guarantee that the level set functions will always remain signed distance functions during the evolution. Numerical errors may be large if the level set functions are not well-behaved. Standard level set techniques are used to keep the level set functions signed distance functions and their zero levels perpendicular to each other. We use the following techniques found in Refs. [20,30–32].

4.2.2.1. Signed distance functions To get a new signed distance function $\tilde{\phi}$ from ϕ, we solve the following evolution equation to steady state:

$$\begin{aligned} &\tilde{\phi}_t + \mathrm{sign}(\phi)(|\nabla\tilde{\phi}| - 1) = 0 \\ &\tilde{\phi}(t = 0) = \phi \end{aligned} \tag{29}$$

where the function $\mathrm{sign}(x)$ is defined by

$$\mathrm{sign}(x) = \begin{cases} -1, & x < 0 \\ 0, & x = 0 \\ 1, & x > 0. \end{cases} \tag{30}$$

Since the signed distance function satisfies $|\nabla\tilde{\phi}| = 1$ and the above evolution equation does not move the zero level of ϕ, theoretically the steady state solution $\tilde{\phi}$ is the desired signed distance function. Similarly, the new signed distance function $\tilde{\psi}$ for the level set function ψ is found by solving the following equation:

$$\begin{aligned} &\tilde{\psi}_t + \mathrm{sign}(\psi)(|\nabla\tilde{\psi}| - 1) = 0 \\ &\tilde{\psi}(t = 0) = \psi. \end{aligned} \tag{31}$$

Numerically, we use the following formulation [31]

$$\begin{aligned} &\tilde{\phi}_t + \frac{\tilde{\phi}}{\sqrt{\tilde{\phi}^2 + |\nabla\tilde{\phi}|^2 \mathrm{d}x^2}}(|\nabla\tilde{\phi}| - 1) = 0 \\ &\tilde{\phi}(t = 0) = \phi. \end{aligned} \tag{32}$$

and

$$\begin{aligned} &\tilde{\psi}_t + \frac{\tilde{\psi}}{\sqrt{\tilde{\psi}^2 + |\nabla\tilde{\psi}|^2 \mathrm{d}x^2}}(|\nabla\tilde{\psi}| - 1) = 0 \\ &\tilde{\psi}(t = 0) = \psi. \end{aligned} \tag{33}$$

We solve for the steady state solutions to these equations using fourth order TVD Runge–Kutta [29] in time and Godunov's scheme [27,33] combined with third order WENO [26] in space. We iterate these equations several steps using half of the Courant–Friedrichs–Levy (CFL) number (i.e. the numerical stability limit) of the fourth order TVD Runge Kutta method [29] as the time increment. We solve for the new level set functions $\tilde{\phi}$ and $\tilde{\psi}$ at each time step for use in solving the evolution equation (16).

4.2.2.2. Perpendicular zero levels Theoretically, the following equation resets the zero level of ϕ perpendicular to that of ψ [20,32]

$$\begin{aligned} &\tilde{\phi}_t + \mathrm{sign}(\psi)\frac{\nabla\psi}{|\nabla\psi|}\cdot\nabla\tilde{\phi} = 0 \\ &\tilde{\phi}(t = 0) = \phi \end{aligned} \tag{34}$$

The numerical formulation is

$$\begin{aligned} &\tilde{\phi}_t + \frac{\psi}{\sqrt{\psi^2 + |\nabla\psi|^2 \mathrm{d}x^2}} \frac{\nabla\psi}{\sqrt{|\nabla\psi|^2 + \mathrm{d}x^2}}\cdot\nabla\tilde{\phi} = 0 \\ &\tilde{\phi}(t = 0) = \phi \end{aligned} \tag{35}$$

We solve for the steady state solution to this equation using fourth order TVD Runge–Kutta [29] in time and third order WENO [26] for the upwind one-sided derivatives of $\tilde{\phi}$. The gradient of ψ in the equation is computed using the average of the third order WENO [26] derivatives on both sides. We iterate this equation several steps using half of the CFL number of the fourth order TVD Runge–Kutta method given in Ref. [29] as the time increment.

Similarly, the following equation resets the zero level of ψ perpendicular to that of ϕ:

$$\begin{aligned} &\tilde{\psi}_t + \mathrm{sign}(\phi)\frac{\nabla\phi}{|\nabla\phi|}\cdot\nabla\tilde{\psi} = 0 \\ &\tilde{\psi}(t = 0) = \psi \end{aligned} \tag{36}$$

and the numerical formulation is

$$\begin{aligned} &\tilde{\psi}_t + \frac{\phi}{\sqrt{\phi^2 + |\nabla\phi|^2 \mathrm{d}x^2}} \frac{\nabla\phi}{\sqrt{|\nabla\phi|^2 + \mathrm{d}x^2}}\cdot\nabla\tilde{\psi} = 0 \\ &\tilde{\psi}(t = 0) = \psi. \end{aligned} \tag{37}$$

We implement it the same way as we do for the equation for $\tilde{\phi}$.

We perform this perpendicular resetting procedure once several time steps for solving the evolution equation (16).

4.2.3. Visualization

The plotting of the dislocation line configurations is complicated by the fact that the dislocation lines are determined implicitly by the two level set functions. We use the following plotting method, described in more detail in Ref. [20]. Each cube in the grid is divided into six tetrahedra. Inside each tetrahedron, the level set functions ϕ and ψ are approximated by linear functions. The intersection of the zero levels of the two linear functions is a line segment inside the tetrahedron

if the intersection is not empty (i.e. we need only compute the two ending points of the line segment on the tetrahedron surface), see Fig. 2. The union of all these segments is the dislocation configuration.

4.2.4. Velocity interpolation and extension

We use a smeared delta function (rather than an exact delta function) to compute the self-stress of the dislocations in order to prevent the self-stress from being singular on the dislocations. The region near the dislocations where the smeared delta function is not equal to zero is the core region of the dislocations. The leading order of the self-stress near the dislocations, when using a smeared delta function, is of the order $1/\varepsilon$, where ε is the dislocation core size. This $O(1/\varepsilon)$ self-stress near the dislocations does not contribute to the motion of the dislocations (it has the effect of expanding the core region). We remove this contribution to the self-stress by a procedure which we call velocity interpolation and extension. We first interpolate the velocity on the dislocation line and then extend the interpolated value to the whole space using the fast sweeping method [34].

In the velocity interpolation, we use a method

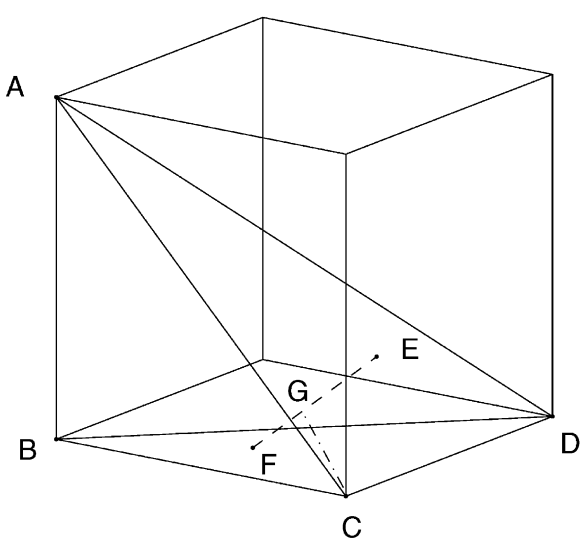

Fig. 2. A cube in the grid, a tetrahedron ABCD and a dislocation line segment EF inside the tetrahedron. Point G is on the segment EF and the length of CG is the distance from the grid point C to the segment EF.

similar to that used in the plotting of dislocation lines. For any grid point, the dislocation line segments in its nearby cubes can be found by the plotting method. The distance from this grid point to the dislocation line is the minimum distance to any dislocation segment. The remainder of the procedure is most simply described by consideration of the example in Fig. 2. The distance from the grid point of interest, point C, to the dislocation line is the distance from C to the segment EF. We can locate a point G on the segment EF, such that the length of CG is the minimum distance from C to EF. We know the velocity on the grid points of the cube in Fig. 2. We compute the velocity on the points E and F by trilinear interpolation of the velocity on these grid points. Then, we compute the velocity on the point G using a linear interpolation of the velocity on E and F. The velocity of point C is approximated as that on grid point G. In summary, velocity interpolation allows us to calculate the velocity associated with any grid point as the velocity of the nearest point on a dislocation segment in adjacent cubes (if one is present).

The trilinear interpolation can be described as follows. Assume we have grid points $(x_{i+l_1}, y_{j+l_2}, z_{k+l_3})$ and the velocity $v_{i+l_1,j+l_2,k+l_3}$ on them, where l_1, l_2, $l_3 = 0, 1$ for some i, j, k. The trilinear interpolation of v on a point (x, y, z) is given by

$$v(x,y,z) = \frac{1}{8} \sum_{l_1,l_2,l_3=0}^{1} v_{i+l_1,j+l_2,k+l_3} \bar{x}_{l_1} \bar{y}_{l_2} \bar{z}_{l_3} \tag{38}$$

where

$$\begin{aligned} \bar{x}_{l_1} &= 1 + (2l_1 - 1)\left(\frac{2(x - x_i)}{\mathrm{d}x} - 1\right) \\ \bar{y}_{l_2} &= 1 + (2l_2 - 1)\left(\frac{2(y - y_j)}{\mathrm{d}y} - 1\right) \\ \bar{z}_{l_3} &= 1 + (2l_3 - 1)\left(\frac{2(z - z_k)}{\mathrm{d}z} - 1\right). \end{aligned} \tag{39}$$

Bilinear and higher order interpolations have been used in other level set method applications [35,36].

To extend the velocities calculated at grid points

neighboring the dislocation lines, we employ the fast sweeping method [34,36–38]. The fast sweeping method is an algorithm for obtaining the distance function to the dislocations at all gridpoints from the distance values (obtained as described above) at gridpoints neighboring the dislocations. Velocity extension is incorporated into this algorithm by updating the velocity at each gridpoint after the distance function is determined such that the velocity is constant in the directions normal to the dislocations (the gradient directions of the distance function).

4.2.5. Initialization

Initially, we choose the level set functions ϕ and ψ such that

1. The intersection of their zero levels gives the initial configuration of the dislocation lines;
2. ϕ and ψ are signed distance functions to their zero levels, respectively;
3. The zero levels of ϕ and ψ are perpendicular to each other.

Though we solve the elasticity equations assuming periodicity, the level set functions are not necessarily periodic and may be defined in a region smaller than the periodic simulation box.

4.3. Outline of the algorithm

Finally, we summarize the steps of our algorithm as follows:

Step 1. Initialize the level set functions ϕ and ψ.
Step 2. Compute the tangent vector ξ and the delta function $\delta(\gamma)$ from the level set functions ϕ and ψ using Eqs. (21) and (28).
Step 3. Compute the self-stress tensor $\{\sigma_{ij}\}$ using Eq. (27) and a FFT.
Step 4. Compute the velocity field using Eqs. (11)–(13).
Step 5. Perform velocity interpolation and extension.
Step 6. Update level set functions ϕ and ψ using Eq. (16).
Step 7. Reinitialize the level set functions ϕ and ψ as signed distance functions at each time step using Eqs. (32) and (33); reset their zero levels perpendicular to each other using Eqs. (35) and (37) after several time steps.
Step 8. Plot the dislocation lines as required for visualization.
Step 9. Repeat step 2 through 8.

5. Examples

In this section, we present several example applications using the level set method for dislocation dynamics proposed above. The simulations were performed within simulation cells that were $l \times l \times l$ (where $l = 2$, except as noted) in arbitrary units. The stresses are scaled by $Gb/2l$, all mobilities are normalized by the glide mobility m_g, and the time is scaled by $4l/Gb^2m_g$, where b is the magnitude of the Burgers vector. We assume period boundary conditions and discretize the simulation cell into $64 \times 64 \times 64$ grid points, except where noted. We set the Poisson ratio $\nu = 1/3$ and the climb mobility $m_c = 0$ except where noted. The simulations described in the next subsection, performed with these parameters, required less than 5 h on a personal computer with a 450 MHz Pentium II microprocessor. The computational efficiency is independent of the absolute value of the glide mobility or the absolute value of the grid spacing.

5.1. Prismatic loop shrinking under its self-stress by climb

At high temperature, a prismatic loop (Burgers vector perpendicular to the plane containing the loop) will shrink under its own self-stress by climb (assuming $m_c > 0$). The leading order term in the force that tends to shrink the loop is [3,22]

$$\frac{Gb^2}{4\pi(1-\nu)}\kappa\log\frac{4}{\varepsilon\kappa} \tag{40}$$

where κ is the curvature of the loop and ϵ is the core radius. For a circular prismatic loop, this is

$$\frac{Gb^2}{4\pi(1-\nu)}\frac{1}{R}\log\frac{4R}{\varepsilon} \tag{41}$$

where R is the radius of the circular loop.

Fig. 3 shows a circular prismatic loop shrinking under its own self-stress by climb. The Burgers vector **b** is in the z direction. (Recall that our choice of Burgers vector is arbitrary and that the orientation of the coordinate system used to describe the simulation cell may be different than the orientation of the traditional crystal coordinate system.) The initial loop is a circle with radius $r = 0.7$ in the x–y plane. We choose time step $dt = 0.0001$ and plot the loop every 100 time steps. Note that the rate at which the loop shrinks increases in time (i.e. with decreasing radius), as expected based upon the driving force dependence on the loop radius (see Eq. (41)). The loop eventually disappears.

5.2. Glide loop expanding under an applied stress

A glide dislocation loop (i.e. a loop in the plane containing the tangent vector of the dislocation and the Burgers vector) will shrink under the action of its self-stress, in the absence of an applied stress.

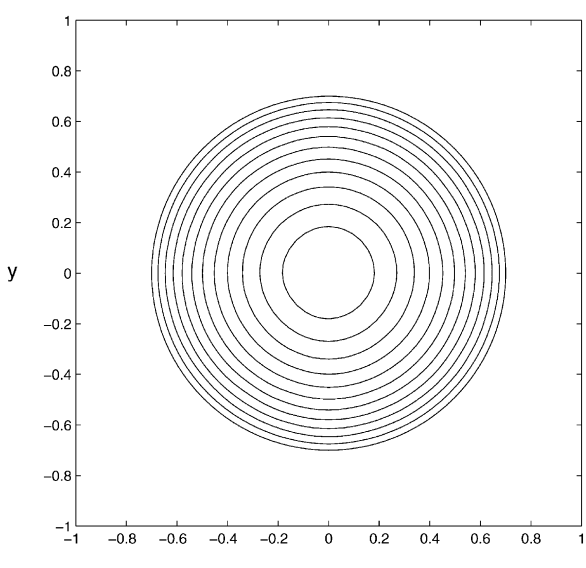

Fig. 3. A prismatic loop shrinking under its self-stress by climb. The Burgers vector **b** is pointing out of the paper. The loop is plotted at uniform time intervals starting with the outermost circle. The loop eventually disappears.

The leading order term in the shrinking force is [3,22]

$$\frac{Gb^2}{4\pi(1-\nu)}[(1+\nu)\cos^2\theta + (1-2\nu)\sin^2\theta]\kappa\log\frac{4}{\varepsilon\kappa} \tag{42}$$

where κ is the curvature of the loop, ε is the core radius, and θ is the angle between the tangent vector of the dislocation and the Burgers vector.

The leading order shrinking force for the pure edge segments of the dislocation loop is

$$\frac{Gb^2}{4\pi}\frac{1-2\nu}{1-\nu}\kappa\log\frac{4}{\varepsilon\kappa}. \tag{43}$$

That for the screw segments of the loop is

$$\frac{Gb^2}{4\pi}\frac{1+\nu}{1-\nu}\kappa\log\frac{4}{\varepsilon\kappa}. \tag{44}$$

For $\nu = 1/3$, the shrinking force on the screw segments exceeds that on the edge segments. Therefore the sections of the loop in the screw orientation shrink faster than those in edge orientations when they have the same curvature.

The glide dislocation loop can expand in its slip plane provided that a sufficiently large external stress is applied. The leading order term in the expansion force is

$$\tau b - \frac{Gb^2}{4\pi(1-\nu)}[(1+\nu)\cos^2\theta + (1-2\nu)\sin^2\theta]\kappa\log\frac{4}{\varepsilon\kappa} \tag{45}$$

where θ is the angle between the tangent vector of the dislocation and the Burgers vector and $\tau = \sigma_{xz}$ is the applied shear stress (see Fig. 4). The expansion force on the screw segments is smaller than that on the edge segments, at fixed curvature and applied stress. Therefore, an initially circular loop should expand slower in the direction parallel to the Burgers vector than in any other direction.

Fig. 4 shows the simulation results for a dislocation loop expanding in its slip plane under an applied stress and the self-stress. The loop is in the x–y plane (the z direction is pointing out of the paper), the Burgers vector **b** is in the x direction

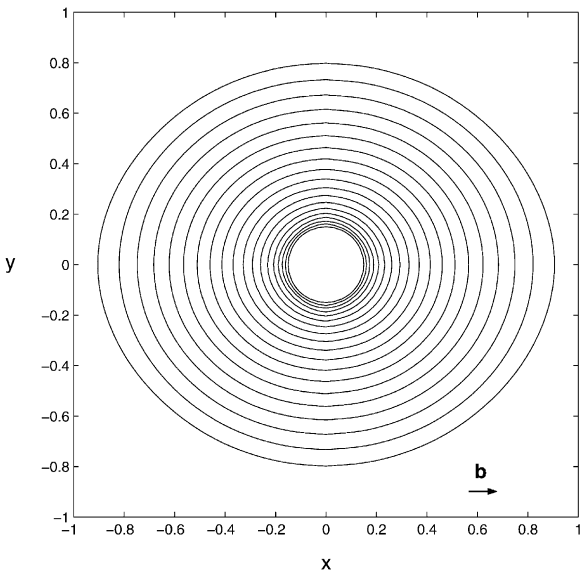

Fig. 4. A dislocation loop with a Burgers vector **b** in the x direction expanding in its slip plane under an applied stress $\sigma_{xz} \neq 0$ (the z direction is pointing out of the paper). The loop is plotted at uniform time intervals starting from the innermost circular loop.

and the tangent vector rotates along the loop in the clockwise direction. The applied shear stress $\sigma_{xz} = 7.5$, while the other components of the applied stress are 0. Initially, the loop is a small circle with radius $r = 0.15$. We choose the time step to be $dt = 0.0001$ and plot the loop every 100 time steps. The loop expands and elongates in the direction of the Burgers vector, as expected based upon the discussion above.

5.3. Dislocation loop expanding under an applied stress: general case

While the previous two cases considered pure climb and pure glide dislocation loop geometries in which the loop remained planar, the evolution of a loop under an arbitrary applied stress need not always move in the initial plane of the loop. Fig. 5(a) shows the expansion of an initially planar, circular loop under the action of an applied stress with non-zero components $\sigma_{xz} = 2.5$, which tends to expand the loop, and $\sigma_{xy} = 4.0$, which tends to move it out of the xy plane. Only the screw segments of the loop move out of the initial plane of the loop. Although there is a finite force on the non-screw oriented segments, they cannot move out of the slip plane because the dislocation mobility in such directions is zero (see Eq. (25)).

At high temperatures, the non-screw components of a dislocation can move out of their slip plane by climb. Fig. 5 shows a simulation of the expansion of the dislocation loop under a range of different climb mobilities. Fig. 5(a) corresponds to the extreme case of $m_c/m_g = 0$. In this case, only the screw part of the dislocation can move out of the slip plane by cross-slip. Fig. 5(e) shows the extreme case of the climb mobility equal to the glide mobility $m_c/m_g = 1$. In this case, the screw segments cross-slip and the non-screw components climb out of the slip plane. The loop appears to rotate as it expands. Fig. 5(b)–(d) show intermediate cases where the degree of climb of the edge components vary.

5.4. Dislocation intersections

We now examine the case of the intersection of pairs of perpendicular dislocation lines for two relatively simple cases. Fig. 6 shows the intersection of a straight edge dislocation with Burgers vector **b** parallel to the x-axis and line direction parallel to the y-axis and another straight edge dislocation with the same Burgers vector and the line direction parallel to the z-axis. The first dislocation line is driven towards the second by an applied stress σ_{xz}. A dislocation reaction occurs when they meet, temporarily joining half of one dislocation with half of the other. As the two halves which originally belonged to the first dislocation continue to move forward, they rejoin and the two halves of what was originally the second dislocation also rejoin. (The level set method represents the two dislocations at the point of intersection by two 90° dislocations. This is equivalent to a pair of perpendicular intersecting dislocations. The choice of representation is arbitrary.) This procedure looks like the first dislocation cutting through the second one. This cutting should produce Burgers vector size kinks in dislocations. However, kinks cannot be resolved in the continuum model. Nonetheless, the barrier to form kinks is reproduced, as indicated

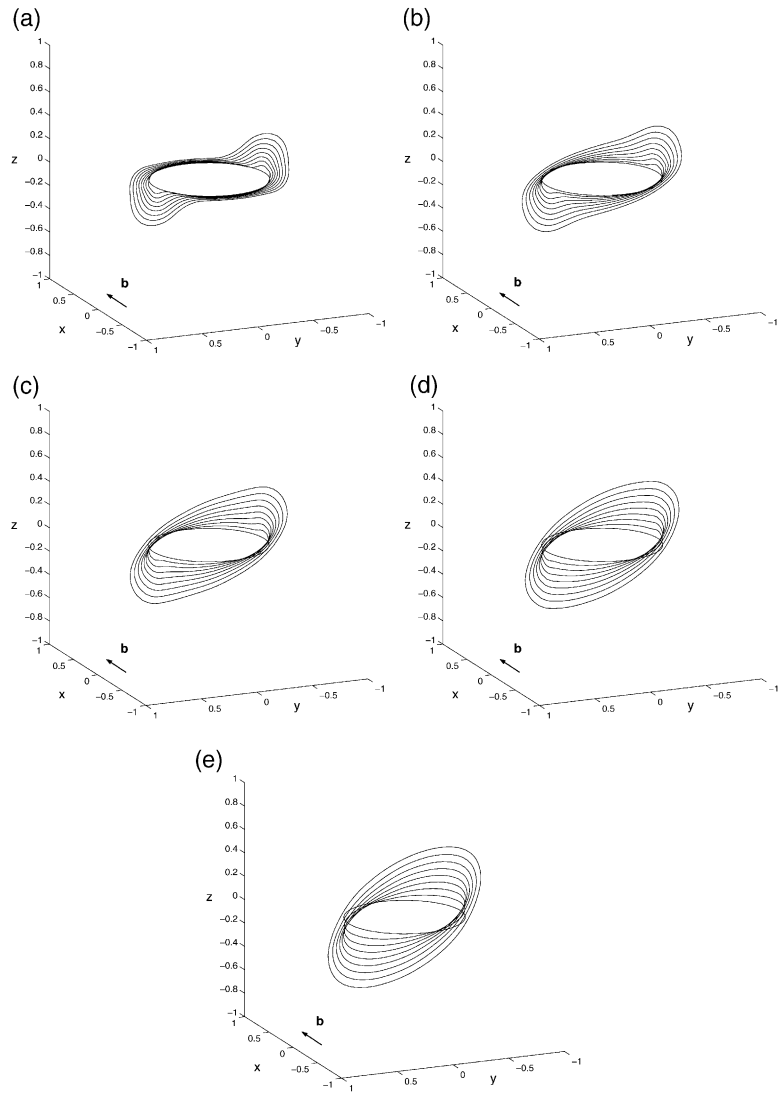

Fig. 5. An initially circular glide loop, with a Burgers vector **b** in the x direction, expanding under a complex applied stress (σ_{xz} = 2.5 and σ_{xy} = 4.0) with mobility ratios m_c/m_g of (a) 0, (b) 0.25, (c) 0.5, (d) 0.75 and (e) 1.0. The loop is plotted at regular intervals in time (every Δt = 0.02).

by the cusps in the dislocation lines formed as one dislocation cuts through the other.

Fig. 7 shows the intersection of two straight screw dislocations with different Burgers vectors $\mathbf{b}_1$ and $\mathbf{b}_2$, respectively. The directions of the two dislocation lines are the same as those in Fig. 6. The Burgers vector $\mathbf{b}_1$ is parallel to the y-axis and the Burgers vector $\mathbf{b}_2$ is parallel to the z-axis. Dislocation 1 moves towards dislocation 2 under the applied stress σ_{yz}. One pair of level set functions is used for each unique Burgers vector (two in this case): dislocation 1—ϕ_1 and ψ_1 and dislocation 2—ϕ_2 and ψ_2. Accordingly, we describe the elastic fields using Eq. (6) rather than Eq. (5). Moving screw dislocation 1 cuts through dislocation 2. In an atomistic view, this cutting operation leaves kinks on each of the screw dislocations, which are not resolved here. The cutting distorts both dislo-

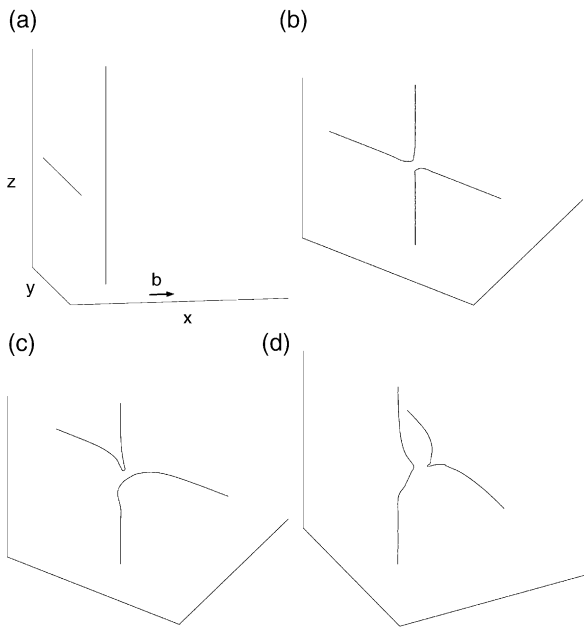

Fig. 6. Intersection of two initially straight edge dislocations with the same Burgers vector **b**. The dislocation that is initially parallel to the *y*-axis, is driven in the +*x*-direction by an applied stress σ_{xz}.

cations and acts as a localized barrier to the motion of dislocation 1.

Admittedly, these two examples are rather simple compared with the types of intersections and junctions (e.g. Lomer locks) that occur in the dynamics of large dislocation ensembles. We will present a more complete analysis of junction formation/dislocation intersections in a subsequent paper.

5.5. Frank–Read source

A Frank–Read source is one of the classic dislocation multiplication mechanisms [39]. We simulate the Frank–Read source in a $4 \times 4 \times 2$ simulation cell that is discretized into $128 \times 128 \times 64$ grid points. The initial configuration is a rectangular loop in the *y*–*z* plane, as shown in Fig. 8(a). The Burgers vector is parallel to the *x*-axis and a stress σ_{xz} is applied. We operate the Frank–Read source under zero climb mobility conditions, such that only the initially horizontal segments are

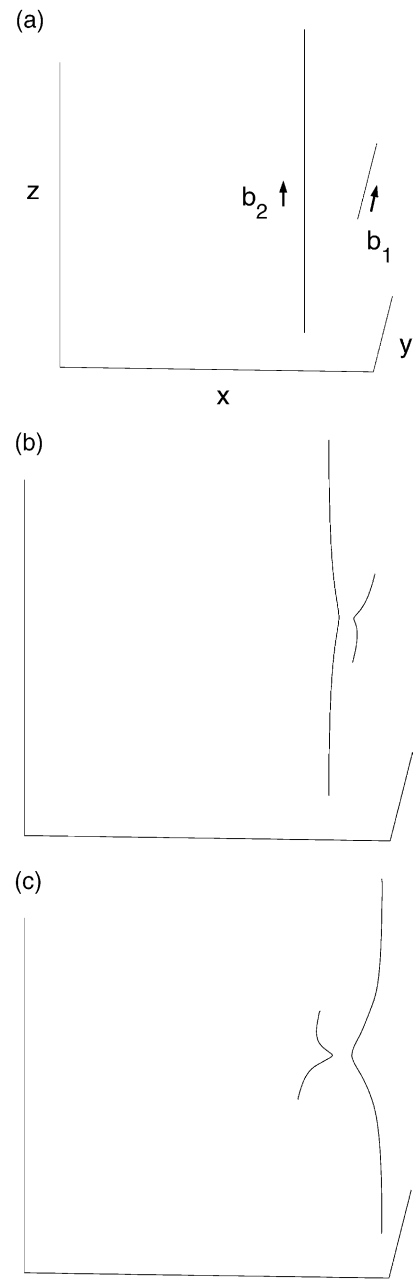

Fig. 7. Intersection of two initially straight screw dislocations with Burgers vectors $\mathbf{b}_1$ and $\mathbf{b}_2$. Dislocation 1 is driven in the direction of the *x*-axis by the applied stress σ_{yz}.

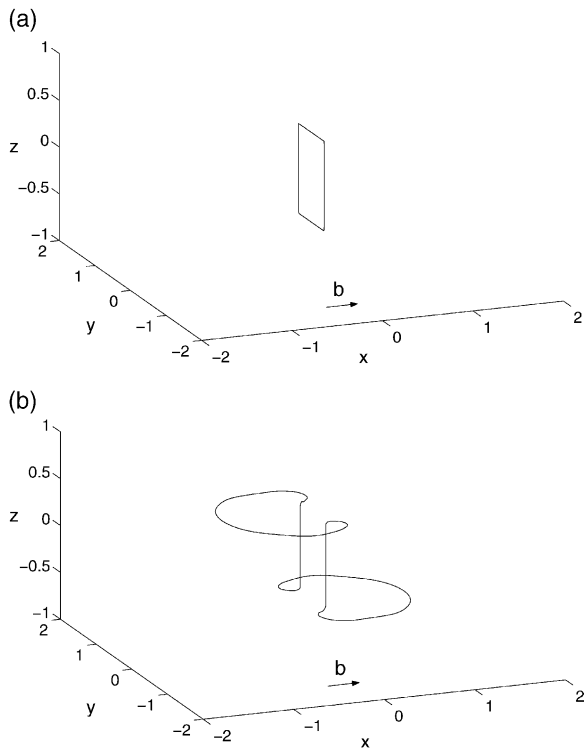

Fig. 8. Frank–Read source. (a) Initial configuration. (b) Configuration after some time.

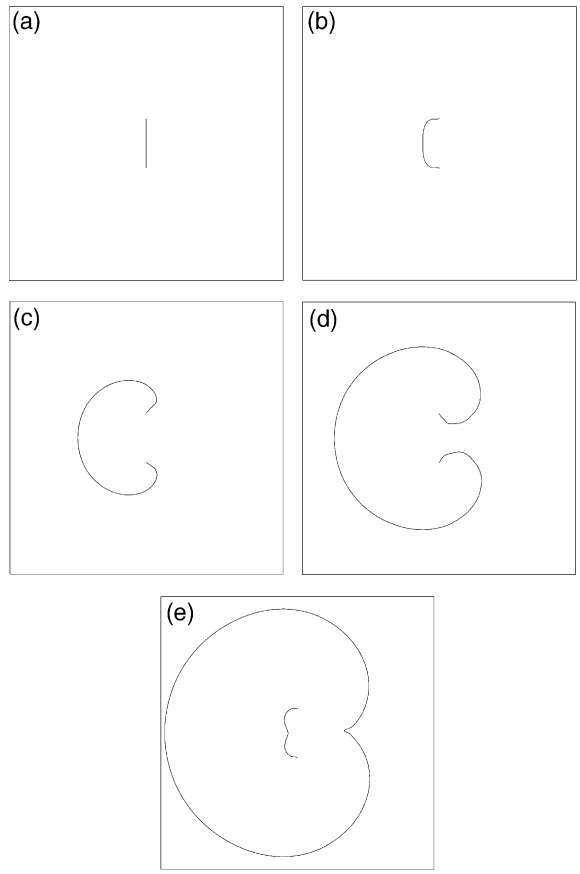

Fig. 9. Simulation of the Frank–Read source. The configuration in the slip plane is plotted at different times during the evolution.

mobile (i.e. the dislocation can glide only in x–y planes). In order to avoid the effects of the very large forces near the corners of the loops, we fix the level set functions near the immobile vertical segments. Fig. 8(b) shows a three-dimensional configuration at some time during the expansion of the Frank–Read source. The evolution of an initially horizontal segment in its slip plane is shown in Fig. 9 (the two end points are pinned). When the stress is applied, the segment increasingly bows out, until opposite sides of the loop meet and annihilate. The meeting and annihilation of opposite sides of the loop is aided by the attractive interaction between these two segments (i.e. which have the same Burgers vector but opposite line direction, ξ). The result of this process is the formation of a large loop with a dislocation segment, similar to the initial one, inside. This segment then bows out under the applied stress and the entire process repeats itself, thus generating a series of concentric dislocation loops.

5.6. Dislocations bypassing particles

We applied the simulation procedure described above to dislocation dynamics in the presence of an array of impenetrable particles. A critical applied stress exists beyond which a dislocation can bypass the array of particles. This is the source of particle strengthening of metals. The value of this critical stress depends upon the particle bypass mechanism. Classically, dislocations can bypass impenetrable particles by either leaving (Orowan) loops behind as the dislocations glide pass the particles [40] or by cross-slip [41,42].

We assume that the particles exert short-range repulsive forces on the dislocations. This short-range repulsive force relaxes the hard core repul-

sion that would occur if the dislocation did not sense the particle until it reached the interface. In nature, such forces are the rule, rather than an exception and can be associated with such phenomena as misfit stresses, interaction associated with elastic heterogeneity or core compression/changes as the dislocation approaches very close to a particle. We assume a repulsive force of the form

$$\frac{A}{(r-B)^3}-C \tag{46}$$

where r is the distance from a point on the dislocation line to the center of the particle. More precisely, for a spherical particle with radius R, we choose a repulsive force with hard core repulsion and a cut-off at large dislocation–particle separation:

$$\begin{cases} +\infty, & \text{if } r \le R/2 \\ \dfrac{Gb^2}{2l}\left(\dfrac{(1.5R)^3}{(r-0.5R)^3}-1\right), & \text{if } R/2 < r \le 2R \\ 0, & \text{if } r > 2R. \end{cases} \tag{47}$$

where we recall that l is the dimension of one edge of the simulation cell.

Numerically, in the velocity interpolation procedure, if there are dislocation segments in the cubes adjacent to a grid point, we compute the repulsive force (Eq. (47)) acting on the nearest point on the dislocation to this grid point and add it to the total force. We then extend the velocity defined near the dislocations to the whole space by velocity extension.

We study the critical applied shear stress for an initially straight dislocation to bypass a regular array of particles. When a dislocation line cannot bypass the particles, it will reach an equilibrium configuration. We assume the equilibrium state is achieved if the averaged velocity of the dislocation v_a over a long time (10,000 time steps in the simulation) is less than 0.002 of the initial velocity of the straight dislocation. The averaged velocity v_a is defined as

$$v_a \equiv \frac{\sum_{|\phi_{ijk}^{(1)}|<dx,\ |\psi_{ijk}^{(1)}|<dx} (|\phi_{ijk}^{(2)}-\phi_{ijk}^{(1)}| + |\psi_{ijk}^{(2)}-\psi_{ijk}^{(1)}|)}{N}, \tag{48}$$

where the subscript ijk is the index of the grid point, $\phi_{ijk}^{(1)}$ and $\psi_{ijk}^{(1)}$ are the values of the level set functions on the grid point ijk at a particular time, $\phi_{ijk}^{(2)}$ and $\psi_{ijk}^{(2)}$ are the values of the level set functions on the grid point ijk at a later time, N is the total number of grid points where $|\phi_{ijk}^{(1)}| < dx$ and $|\psi_{ijk}^{(1)}| < dx$. A similar definition of the equilibrium state was used in level set method calculations of two dimensional, multiphase motion [38].

5.6.1. Bypassing mechanisms

5.6.1.1. Orowan mechanism Fig. 10 shows a simulation of an edge dislocation bypassing a linear array of spherical particles that are coplanar. The dislocation approaches the particle array and then bows out between the particles. The two dislocation segments on the sides of the particle are elastically attracted to each other (recall that they

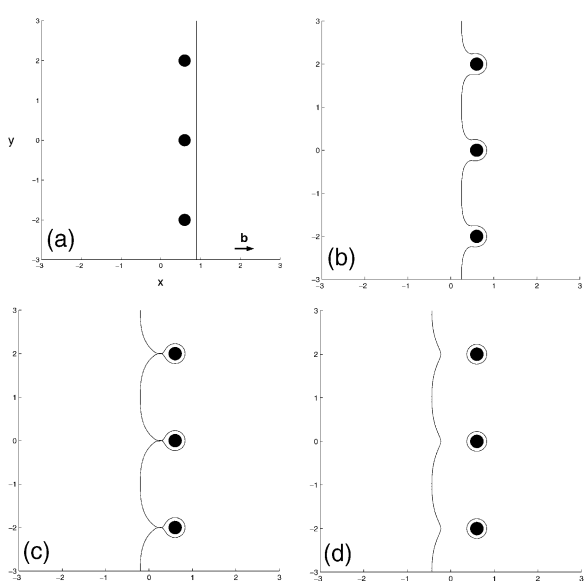

Fig. 10. An edge dislocation bypassing a linear array of particles, leaving Orowan loops around the particles behind. The Burgers vector **b** is in the x direction. The applied stress $\sigma_{xz} \neq 0$, where the z direction is pointing out of the paper. The glide plane of the dislocation intersects the centers of the particles.

have the same Burgers vector but opposite line directions). These two segments annihilate one another, leave behind a dislocation loop as the dislocation moves on. This is exactly the classical Orowan [40] mechanism for bypassing particles. Similar simulation results were obtained for a screw dislocation bypassing a linear array of spherical particles in the same plane.

5.6.1.2. Cross-slip In 1957, Hirsch suggested [41] that dislocations can also bypass particles by cross-slip. A detailed description of this mechanism was provided by Hirsch and Humphreys [42]. We examined this cross-slip bypassing mechanism using our level set method. Figs. 11 and 12 show such a bypass process for the case in which the plane along which the dislocation would glide in the absence of particles does not contain the centers of the particles.

Fig. 11 shows an edge dislocation bypassing a particle by cross-slip. The edge dislocation approaches the particle under the action of the applied stress. The dislocation begins bowing between the particles until two segments are oriented perpendicular to the initial line direction. These segments are screws. The screw segments cross-slip over the top of the particle and annihilate each other there. Since the edge segments cannot cross-slip, a non-glide loop is left behind the particle. The resultant loop is canted with respect to the loops in Fig. 10 (i.e. where the particle center and dislocation are exactly coplanar such that there is no glide force out of the plane).

Fig. 12 shows a screw dislocation bypassing a particle by a combination of Orowan looping and cross-slip. The screw dislocation approaches the particle under the action of the applied stress and begins to bend around the particle. The segments that begin to bend have at least partial edge character and cannot cross-slip. On the other hand, the segment behind the particle, remains in screw orientation and begins to cross-slip over the particle under the applied stress and its interaction with the non-coplanar particle. At the same time, the dislocation continues to bend around the particle and pinches-off an Orowan loop. Since this loop does not lie in the plane containing the particle center, the screw segment formed when the

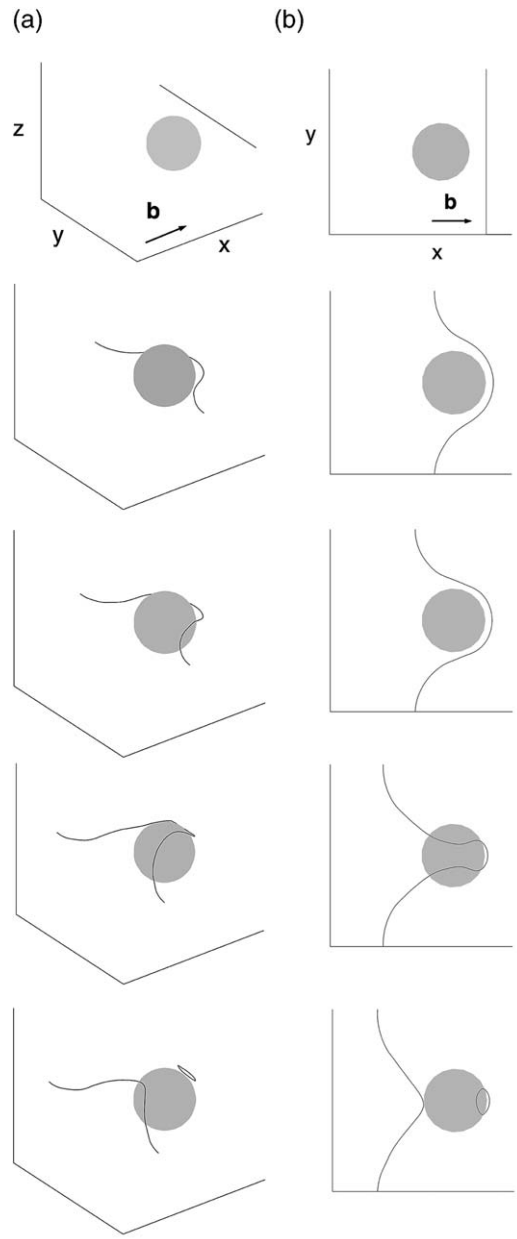

Fig. 11. An edge dislocation bypassing a particle by the Hirsch mechanism through cross-slip. The top set of panels show a three-dimensional view, while the bottom set is viewed from above (i.e. looking in the $-z$ direction). The Burgers vector **b** is in the x direction, the applied stress is $\sigma_{xz} \neq 0$, and the initial edge dislocation glide plane is above (in the $+z$ direction) the particle center.

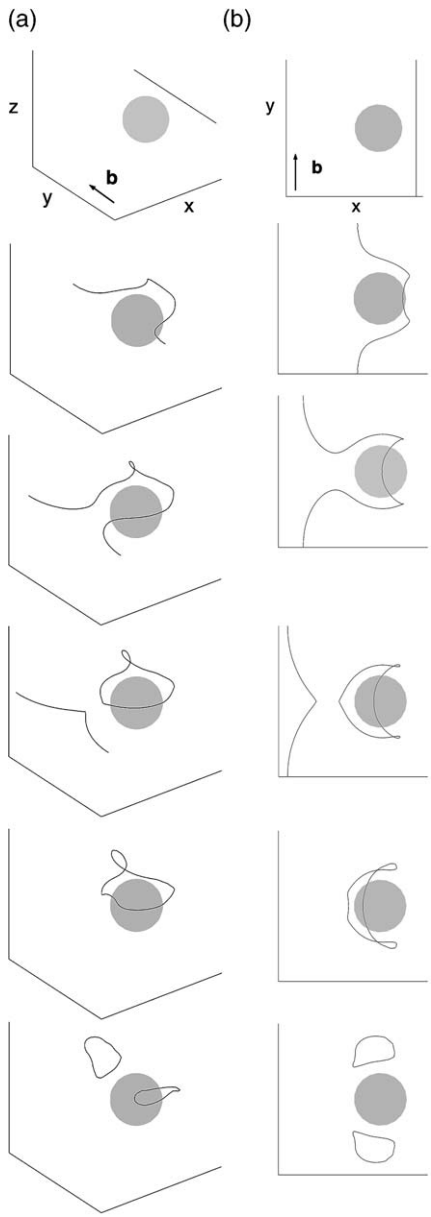

Fig. 12. A screw dislocation bypassing a particle by a combination of Orowan looping and cross-slipping. The top set of panels show a three-dimensional view, while the bottom set is viewed from above (i.e. looking in the $-z$ direction). The Burgers vector **b** is in the y direction, the applied stress is $\sigma_{yz} \neq 0$, and the plane in which the screw dislocation would glide in the absence of the particle is above the particle center (in the $+z$ direction).

Orowan loop pinches-off begins cross-slipping over the top of the particle. The screw segments from in front of and behind the particle are attracted toward each other and annihilate. This leaves behind two dislocation loops on the two sides of the particle. These are non-glide loops.

Our simulations agree with and confirm the prediction of the cross-slip bypassing theory.

5.6.2. Critical applied stress

In addition to showing the bypass mechanism, a successful method for simulating dislocation motion should also be able to quantitatively predict the critical applied shear stress for a dislocation to bypass a particle array. We examined the critical stress for an edge dislocation bypassing an array of spherical particles of diameter $D = 0.2$ that is periodic in the x, y and z directions. The initial straight dislocation is parallel to the y direction and has a Burgers vector in the x direction. The bypass criterion was as described at the beginning of this section. We performed a series of simulations, in which we varied the applied stress in a binary search to determine the critical applied stress. Simulations were performed for several values of the inter-particle separation L, see Fig. 13.

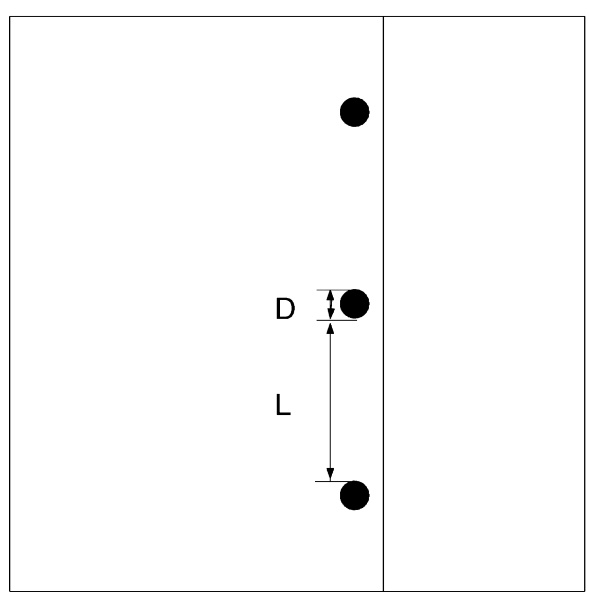

Fig. 13. A schematic illustration of the geometry used to determine the critical applied stress. The inter-particle separation L and the particle diameter D are indicated.

The critical stress for an edge dislocation to bypass the particles by the Orowan mechanism can be approximated as [17,40,43]

$$\tau \approx \frac{Gb}{2\pi L}\log\frac{D_1}{r_0} \tag{49}$$

where D_1 is the harmonic mean of L and D

$$D_1 = (D^{-1} + L^{-1})^{-1} \tag{50}$$

and r_0 is the inner cut-off radius, associated with the dislocation core.

Fig. 14 shows the critical stress required for the dislocation to bypass the particle array (in units of Gb/L) versus $\log(D_1/r_0)$ The data points represent the simulation results and the straight line is the best fit to our data using Eq. (49).[1] Excellent agreement between our simulation results and the theoretical estimate is achieved. This suggests that the proposed dislocation dynamics simulation procedure can be employed to make quantitative predictions.

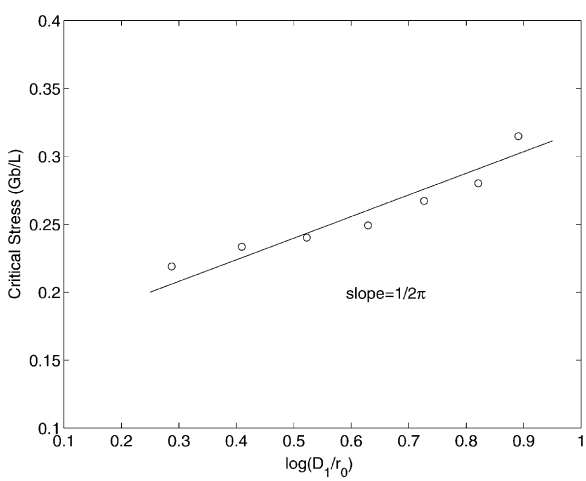

Fig. 14. The critical stress plotted in the unit Gb/L against $\log(D_1/r_0)$.

[1] Due to the detailed form we chose for the repulsive interaction between dislocations and particles (Eq. (47)), the effective diameter of the particles is $D = 0.26$, rather than $D = 0.2$.

6. Summary

We have proposed a novel three-dimensional level set method for dislocation dynamics, in which the dislocation lines are represented by the intersection of the zero levels of two three-dimensional level set functions. The evolution of the dislocation lines is implicitly determined by the evolution of the two level set functions. Linear elasticity theory is used to compute the elastic interactions between dislocations. The equations describing the elastic behavior were solved using the fast Fourier transform FFT method with periodic boundary conditions.

Since the level set method does not directly track the motion of individual dislocation line segments, it can easily handle topological changes that readily occur during the evolution of dislocation microstructures. Our level set method naturally incorporates inherently three-dimensional motion of dislocations, thereby accounting for cross-slip and climb. Relative glide and climb mobilities can be fixed arbitrarily, as necessary for capturing temperature-dependent behavior. Numerical implementation of the level set method was through simple and accurate finite difference schemes on uniform grids.

Simulation examples using our method show the glide, cross-slip and climb of dislocation loops under applied and/or self-stresses, the intersection of dislocation lines, and the operation of a Frank–Read source. In the presence of impenetrable particles, our simulations show that the dislocation can bypass the particles by Orowan loop mechanism or the combination mechanisms of Orowan loop and cross-slip. An example of the relationship of the critical bypassing applied stress against the particle size and inter-particle distance is quantitatively studied. All these simulation results agree very well with the theoretic predictions and the results obtained using other methods.

Acknowledgements

The authors gratefully acknowledge useful discussions with Prof. Stanley Osher (UCLA). This work was supported by the National Science Foun-

dation through grant DMR0080766 and the Defense Advanced Research Project Agency through grant F33615-01-2-2165. The second author was supported in part by NSF Grant #0208449.

References

[1] Volterra V. Ann Ec Norm 1905;24:401.
[2] Nabarro FRN. Theory of crystal dislocations. Oxford, England: Clarendon Press, 1967.
[3] Hirth JP, Lothe J. Theory of dislocations, 2nd ed. New York: John Wiley, 1982.
[4] Kubin LP, Canova GR. In: Messerschmidt U, editor. Electron microscopy in plasticity and fracture research of materials. Berlin: Akademie Verlag; 1990:23.
[5] Kubin LP, Canova G, Condat M, Devincre B, Pontikis V, Brechet Y. Solid State Phenomena 1992;23/24:455.
[6] Zbib HM, Rhee M, Hirth JP. Int J Mech Sci 1998;40:113.
[7] Rhee M, Zbib HM, Hirth JP, Huang H, de la Rubia T. Model Simul Mater Sci Eng 1998;6:467.
[8] Schwarz KW. J Appl Phys 1999;85:108.
[9] Ghoniem NM, Tong SH, Sun LZ. Phys Rev B 2000;61:913.
[10] Khachaturyan AG. In: Turchi EA, Shull RD, Gonis A, editors. Science of alloys for the 21st Century, TMS Proceedings of a Hume–Rothery Symposium. TMS; 2000:293.
[11] Wang YU, Jin YM, Cuitino AM, Khachaturyan AG. Acta Mater 2001;49:1847.
[12] Weygand D, Friedman LH, Van der Giessen E, Needleman A. Model Simul Mater Sci Eng 2002;10:437.
[13] Pant P, Schwarz KW, Baker SP. Acta Mater 2003;51:3243.
[14] Peach M, Koehler JS. Phys Rev 1950;80:436.
[15] Foreman AJE, Makin MJ. Phil Mag 1966;14:911.
[16] Bacon DJ. Physica Status Solidi 1967;23:527.
[17] Bacon DJ, Kocks UF, Scattergood RO. Phil Mag 1973;28:1241.
[18] Devincre B, Kubin LP, Lemarchand C, Madec R. Mat Sci Eng A-Struct 2001;309:211.
[19] Osher S, Sethian JA. J Comput Phys 1988;79:12.
[20] Burchard P, Cheng LT, Merriman B, Osher S. J Comput Phys 2001;170:720.
[21] Osher S, Fedkiw RP. J Comput Phys 2001;169:463.
[22] Lardner RW. Mathematical theory of dislocations and fracture. Toronto and Buffalo: University of Toronto Press, 1974.
[23] Landau LD, Lifshitz EM. Theory of elasticity, 3rd ed. New York: Pergamon Press, 1986.
[24] Bulatov VV, Rhee M, Cai W. In: Kubin L, et al., editor. Multiscale modeling of materials—2000. Warrendale, PA: Materials Research Society; 2001.
[25] Cai W, Bulatov VV, Chang J, Li J, Yip S. Phil Mag 2003;83:539.
[26] Jiang GS, Peng D. SIAM J Sci Comput 2000;21:2126.
[27] Osher S, Shu CW. SIAM J Numer Anal 1991;28:907.
[28] Shu CW, Osher S. J Comput Phys 1988;77:439.
[29] Spiteri RJ, Ruuth SJ. SIAM J Numer Anal 2002;40:469.
[30] Sussman M, Smereka P, Osher S. J Comput Phys 1994;114:146.
[31] Peng D, Merriman B, Osher S, Zhao HK, Kang M. J Comput Phys 1999;155:410.
[32] Osher S, Cheng LT, Kang M, Shim H, Tsai YHR. J Comput Phys 2002;179:622.
[33] Bardi M, Osher S. SIAM J Math Anal 1991;22:344.
[34] Tsai YHR, Cheng LT, Osher S, Zhao HK, UCLA CAM Report 01-27, SIAM J Numer Anal 2003;41:673.
[35] Hou TY, Li Z, Osher S, Zhao HK. J Comput Phys 1997;134:236.
[36] Chen S, Merriman M, Osher S, Smereka P. J Comput Phys 1997;135:8.
[37] Adalsteinsson D, Sethian JA. J Comput Phys 1999;148:2.
[38] Zhao HK, Chan T, Merriman B, Osher S. J Comput Phys 1996;127:179.
[39] Frank FC, Read WT. In: Symposium on plastic deformation of crystalline solids. Pittsburgh: Carnegie Institute of Technology, 1950 44.
[40] Orowan E. In: Symposium on internal stress in metals and alloys. London: The Institute of Metals, 1948 451.
[41] Hirsch PB. J Inst Met 1957;86:13.
[42] Hirsch PB, Humphreys FJ. In: Argon AS, editor. Physics of strength and plasticity. Cambridge: MIT Press; 1969.
[43] Ashby MF. Acta Metall 1966;14:679.